EASL CONGRESS
Vienna, Austria
21–24 June 2023

Immune cell incompetence and hepatocyte differentiation defects explain mild fibrosis in a model of Alagille syndrome

Jan Mašek[1,2*], Iva Filipovic[3☯], Simona Hankeová[1☯], Jingyan He[1☯], Noémi Van Hul[1], Lenka Belicová[1], Anna Maria Frontino[2], Fabio Turetti[2], Igor Červenka[1], Lenka Sarnová[4], Markéta Jiroušková[4], Daniel Oliveira[2], Tomáš Brabec[2], Martin Gregor[4], Niklas Björkström[3], Jan Dobeš[2], Emma R. Andersson[1*]

*correspondence to jan.masek@natur.cuni.cz and/or emma.andersson@ki.se ☯equal contribution

Affiliation:
[1] Department of Cell and Molecular Biology, Karolinska Institute, Stockholm, SE-171 77 Solna, Sweden.
[2] Department of Cell Biology, Faculty of Science, Charles University, Viničná 7, 128 00 Prague 2, Czech Republic.
[3] Center for Infectious Medicine, Department of Medicine Huddinge, Karolinska Institutet, Karolinska University Hospital, Stockholm, Sweden
[4] Laboratory of Integrative Biology, Institute of Molecular Genetics of the Czech Academy of Sciences, Vídeňská 1083, Prague, Czech Republic.

Introduction

Alagille syndrome (OMIM 118450; ALGS) is a multisystemic pediatric genetic disorder characterized by bile duct paucity and multiple associated symptoms present with different penetrance [1,2]. It is in majority of cases (~94%) caused by a mutation in Notch pathway ligand JAGGED1 (JAG1) [3–5], and to lesser extent by the NOTCH2 [4]. Chronic liver diseases are a key risk factor of hepatocellular carcinoma (HCC), fueling the required preceding steps of chronic hepatitis, fibrosis and cirrhosis, and a Notch "ON" signature was found in ~30% of HCC patients [6]. The role of JAG1 in these processes is unclear, only 56% of patients with ALGS and HCC had underlying fibrosis [7].

Interestingly, fibrosis in ALGS, when present, is atypical, with a perisinusoidal and/or pericellular "chicken-wire" appearance, rather than bridging fibrosis [8], suggesting the inflammation-fibrosis-cirrhosis-HCC axis is disrupted in ALGS. Further, only approximately 12-14% of Alagille patients develop cirrhosis, but only <1% HCC [7], or if the loss of functional JAGGED1 confer some protection against HCC. Notch regulates liver and immune system development, and immune system is compromised in patients with ALGS [9], but how these interact in ALGS is unknown.

Aim

Investigate the effects of Jag1 hypomorphism on the immune system, fibrosis, and liver disease progression.

Method

- Mice - *Jag1*$^{+/Ndr}$ mice were outbred to a C3H/C57bl6 background to produce a model for ALGS, dissociated liver tissue from P3 pups was used both for sc-RNA-seq and FACS analysis.
- Bulk and Single-cell RNA sequencing using Chromium 10x platform and analysis in Seurat packages following the ScTransform and Anchoring pipelines [11].
- 25-colour flow cytometry analysis on BD FACSymphony cytometer was followed by high-dimensional post-processing using UMAP and PhenoGraph.
- Adaptive immune cell transfer followed by recovery model of Dextran Sodium Sulphate (**DSS**)-induced chronic ulcerative colitis; experimentally-induced cholestasis: (i) 3,5-diethoxycarbonyl-1,4-dihydrocollidine (**DDC**)-induced primary sclerosing cholangitis, and (ii) bile duct ligation (**BDL**), a surgically-induced obstructive cholestasis.

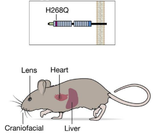

Andersson et al., 2018 [10]

Conclusions

Jag1 regulates hepatocyte differentiation, immune cell development and competence, and *Jag1*$^{Ndr/Ndr}$ lymphocytes specifically inhibit biliary damage-induced periportal fibrosis, providing a mechanistic explanation of atypical fibrosis in ALGS. Transcriptomic analyses corroborate dampened inflammation, fibrosis and cirrhosis in patients with ALGS, as well as a low liver cancer signature compared to other liver diseases. In conclusion, Jag1 regulates immune system interaction with liver injury to modulate fibrosis in an insult-specific manner.

Results

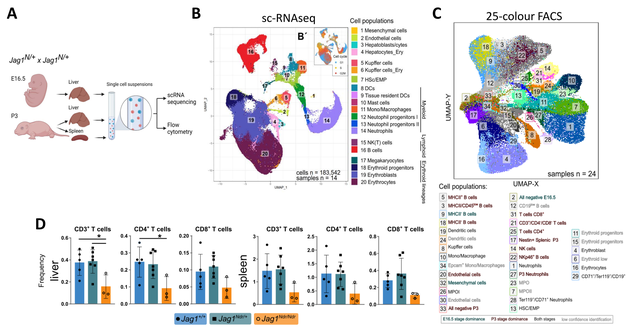

Single cell analyses reveals a reduction in T-cells in *Jag1*$^{Ndr/Ndr}$ liver. (**A**) Experimental schematic. Livers were collected at E16.5 or P3, and spleens were collected at P3. (**B**) UMAP projection of the 183,542 sequenced cells in cell type-annotated clusters, and cell cycle phase (B'). (**C**) UMAP projection of randomly selected 190,000 cells analyzed by 25-color FACS with cell type-annotated clusters from E16.5 and P3 livers, and P3 spleens of *Jag1*$^{+/+}$(n=7), *Jag1*$^{Ndr/+}$(n=11), and *Jag1*$^{Ndr/Ndr}$ (n=6) animals. (**D**) Relative frequency of the CD3$^+$, CD4$^+$/CD3$^+$, and CD8$^+$/CD3$^+$ T-cells in livers and spleens from the *Jag1*$^{+/+}$, *Jag1*$^{+/Ndr}$ and *Jag1*$^{Ndr/Ndr}$ mice at P3.

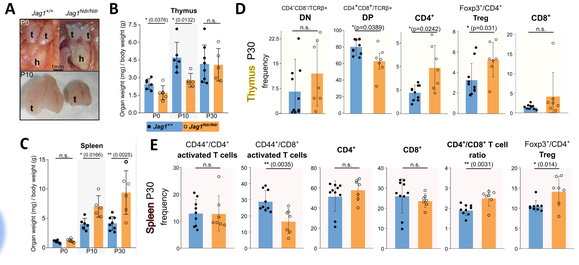

Enrichment of CD4$^+$ and Treg cells at the expense of cytotoxic CD8$^+$ T-cells in *Jag1*$^{Ndr/Ndr}$ mice. (**A**) Macroscopic images of *Jag1*$^{+/+}$ and *Jag1*$^{Ndr/Ndr}$ thymi at P0 and P10. (**B,C**)Thymic and splenic (**B**) weights at P0, P10,and P30 normalized to body weight. (**D, E**) FACS analysis of cell frequencies of different thymic (D), and splenic T-cell (E) populations isolated from *Jag1*$^{+/+}$ and *Jag1*$^{Ndr/Ndr}$ mice at P30.

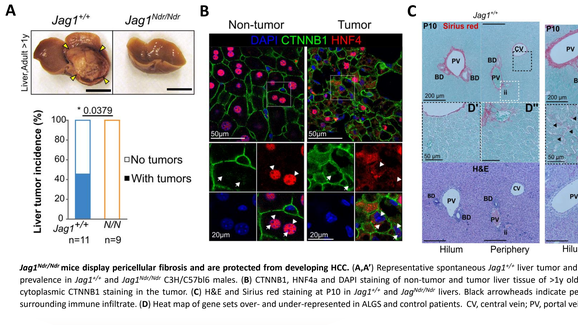

***Jag1*$^{Ndr/Ndr}$ mice display pericellular fibrosis and are protected from developing HCC.** (**A,A'**) Representative spontaneous *Jag1*$^{+/+}$ liver tumor and a tumor-free *Jag1*$^{Ndr/Ndr}$ liver, with quantification of liver tumor prevalence in *Jag1*$^{+/+}$ and *Jag1*$^{Ndr/Ndr}$ C3H/C57bl6 males. (**B**) CTNNB1, HNF4a and DAPI staining of non-tumor and tumor liver tissue of >1y old *Jag1*$^{+/+}$ mice. Arrowheads indicate nuclei, and arrows indicate cytoplasmic CTNNB1 staining in the tumor. (**C**) H&E and Sirius red staining at P10 in *Jag1*$^{+/+}$ and *Jag*$^{Ndr/Ndr}$ livers. Black arrowheads indicate pericellular and periportal fibrosis, white arrowheads fibrosis surrounding immune infiltrate. (**D**) Heat map of gene sets over- and under-represented in ALGS and control patients. CV, central vein; PV, portal vein; BD, bile duct; ii, immune cell infiltrate.

***Jag1*$^{Ndr/Ndr}$ hepatocyte differentiation is delayed, reducing their activation by cholestasis.** (**A**) UMAP projections of the 03_Hepatoblast/cytes and 04_Hepatocytes_Ery subsets. (**B**) Feature plots with localization of (*Epcam*, *Sox9*, *Spp1*), hepatocyte (*Dlk1*, *Hnf4a*, *Alb*, *Afp*), and B-cell (*Cd19*, *Pax5*) marker mRNA expression. (**C**) Average proportion of hepatic cell types per stage and genotype normalized to the number of cells per sample. (**D, E**) Whole liver cell populations (D), and stage-specific hepatocyte expression profile (E) identified in P10 whole liver *Jag*$^{Ndr/Ndr}$ and *Jag1*$^{+/+}$ bulk RNA seq after deconvolution, with MuSiC. (**F**) Violin plots of Egr1-induced proinflammatory genes in hepatocytes. (**G**) Heat map of Egr1-induced proinflammatory genes expressed by hepatocytes in *Jag1*$^{Ndr/Ndr}$ and *Jag1*$^{+/+}$ mice at P10. (*, p_{adj} <0.01, Log2 FC>0.5).

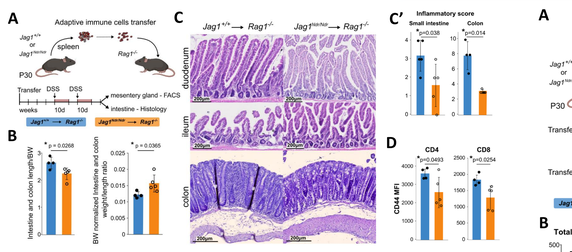

***Jag1*$^{Ndr/Ndr}$ lymphocyte inflammatory response to bacterial infection in an Ulcerative colitis model is deficient.** (**A**) Scheme of the DSS-induced ulcerative colitis experimental model. (**B**) Combined length, and weight/length ratios of the *Jag1*$^{+/+}$→*Rag1*$^{-/-}$ and *Jag1*$^{Ndr/Ndr}$→*Rag1*$^{-/-}$ intestines and colons normalized to BW. (**C,C'**) Representative H&E-stained intestinal (top), and colonic (bottom) sections from the *Jag1*$^{+/+}$ or *Jag1*$^{Ndr/Ndr}$ T-cell-transferred *Rag1*$^{-/-}$ mice after the DSS treatment (C), and their inflammatory scores (C'). (**D**) FACS analysis of the mean fluorescence intensity (MFI) of CD44 staining of CD4$^+$ and CD8$^+$ T-cells from *Jag1*$^{+/+}$→*Rag1*$^{-/-}$ and *Jag1*$^{Ndr/Ndr}$→*Rag1*$^{-/-}$ mesentery glands. # - artefact.

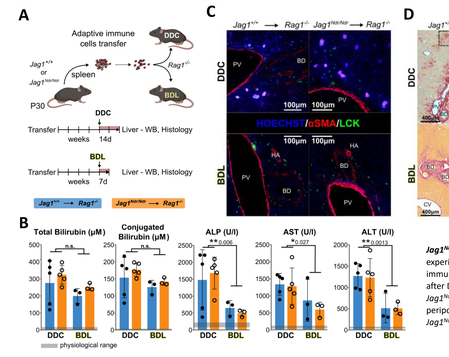

***Jag1*$^{Ndr/Ndr}$ T-cells limit the extent of BDL-induced, but not DDC-induced, periportal fibrosis.** (**A**) Scheme of the parallel DDC and BDL experimental models. (**B**) Liver biochemistry of the *Jag1*$^{+/+}$→*Rag1*$^{-/-}$ and *Jag1*$^{Ndr/Ndr}$→*Rag1*$^{-/-}$ mice after DDC or BDL. (**C**) Representative immunofluorescent images of cryosections from the left lateral lobe (LLL) of *Jag1*$^{+/+}$→*Rag1*$^{-/-}$ (left) and *Jag1*$^{Ndr/Ndr}$→*Rag1*$^{-/-}$ (right) mice after DDC or BDL, stained with α-Lck and α-SMA. (**D**) Representative images of paraffin sections from the LLL of *Jag1*$^{+/+}$→*Rag1*$^{-/-}$ (left) and *Jag1*$^{Ndr/Ndr}$→*Rag1*$^{-/-}$ (right) after the DDC or BDL, stained with Sirius red (SR), and quantification. (**E**) Quantification of SR staining in periportal areas of *Jag1*$^{+/+}$→*Rag1*$^{-/-}$ and *Jag1*$^{Ndr/Ndr}$→*Rag1*$^{-/-}$ livers after BDL and CK19, SMA, and Collagen1 staining of *Jag1*$^{+/+}$→*Rag1*$^{-/-}$ and *Jag1*$^{Ndr/Ndr}$→*Rag1*$^{-/-}$ livers after BDL, and signal quantification in periportal areas.

Acknowledgements

CIMED CENTER FOR INNOVATIVE MEDICINE
Wenner-Gren Stiftelserna
EASL Sheila Sherlock Post Graduate Fellowship Program
PRIMUS
JUNIOR Fund
STARS
Co-funded by the European Union
MINISTRY OF EDUCATION, YOUTH AND SPORTS

References

1. Alagille et al. J. Pediatr. 86, (1975).
2. Mašek et al. Development 144, (2017).
3. Oda et al. Nat. Genet. 16, (1997).
4. McDaniell et al. Am. J. Hum. Genet. 79, (2006).
5. Li et al. Nat Genet 16, (1997).
6. Villanueva et al. Gastroenterology 143, (2012).
7. Vandriel et al., Hepatology, (2022)
8. Fabris et al., Am. J. Pathol. , (2007)
9. Shamoun et al., Clin. Res. Hepatol. Gastroenterol., (2015)
10. Andersson et al. Gastroenterology 154, (2018).
11. Butler et al., Nat. Biotechnol., (2018)
12. Wang et al., Nat. Commun., (2019)
13. Liang et al., Dev. cell, (2022)

Contact

Jan Mašek | PhD
maseklab.org
#JanMasekLab
jan.masek@natur.cuni.cz

Poster Session Online
Scan to download the poster
DOI: 10.3252/pso.eu.EASLCONGRESS.2023
EASL CONGRESS Vienna, Austria 21-24 June 2023
General Hepatology
Jan Maek
THU–255
EASL2023